JOURNAL OF MATERIALS SCIENCE 37 (2002) 1387–1394

Microstructure and mechanical properties of ZrO_2-Gd_2O_3 tetragonal polycrystals

S. BHATTACHARYYA, D. C. AGRAWAL
Materials Science Programme, Indian Institute of Technology, Kanpur 208016, India
E-mail: agrwald@iitk.ac.in

The phases, transformability, microstructure and mechanical properties of ZrO_2-Gd_2O_3 polycrystals containing 1.75–8 mol% Gd_2O_3 were studied. The samples were prepared by a coprecipitation route followed by sintering at 1400°C for 2 hours. The grain size was in the range of 0.1–0.2 μm except for some large grains at high Gd_2O_3 contents. Only a tetragonal phase was observed between 2–4 mol% Gd_2O_3 and a cubic phase for compositions containing $\geq$9.6 mol% Gd_2O_3. A peak K_{IC} of 12 MPa $m^{1/2}$ and a strength of 800 MPa were obtained in the 2 mol% Gd_2O_3 alloy for which the t $\rightarrow$ m transformation on the fracture surface was also found to be maximum. Transformation toughening is able to account for most of the toughness of the samples.

1. Introduction

The stabilization of the tetragonal phase in ZrO_2 by rare earth oxides such as CeO_2, Gd_2O_3, Er_2O_3 and Yb_2O_3 is well documented. However, except for CeO_2, other additives have not received much attention, perhaps because of the difficulty in preparation of powders which sinter to a high density yielding a tetragonal phase with high transformability under stress. CeO_2 stabilized tetragonal zirconia polycrystal (Ce-TZP) has been quite extensively studied, next only to Y_2O_3 stabilized tetragonal zirconia polycrystal (Y-TZP). In spite of the high K_{IC} and strength of these TZP's, their use is restricted because of the problem of degradation of properties due to t $\rightarrow$ m transformation when held at low temperatures (200–500°C) [1]. Thus it is of interest to study the preparation and properties of ZrO_2 stabilized by other additives.

Out of the potential rare earth stabilizers, Er_2o_3 leads to high sintered density but the t phase is highly stable against transformation [2]. The ZrO_2-Gd_2O_3 has been studied by many investigators though not with a view to design Gd-TZP with good mechanical properties. Van Dijk *et al*. [3] prepared ZrO_2-Gd_2O_3 solid electrolytes and measured their electrical conductivity. Similar studies have also been reported by Moztarzadeh [4] and Kang *et al*. [5]. Michel *et al.* [6] prepared Gd_2O_3 doped tetragonal zirconia single crystals by skull melting for studying their fracture behaviour and Leung *et al.* [7] studied the high temperature phase partitioning in ZrO_2-Gd_2O_3 system prepared from aqueous precursors.

One important consideration in the use of stabilized zirconias is their degradation behaviour at low temperatures. The kinetics of low temperature aging is believed to be dependent on the strain in the zirconia lattice [8]. As Gd^{3+} has an ionic radius (0.96 Å) [9] closer to Zr^{4+} (0.87 Å), than Y^{3+} (1.06 Å), it is conceivable that stabilization by Gd^{3+} could lead to lower strain in the lattice and thereby lower aging rates. Moreover, the high rate of partitioning of Gd_2O_3 between the t and c phases [7] should make it much easier to tailor the microstructure to different applications. With this in view, we have studied the phases, t $\rightarrow$ m transformability, microstructure and mechanical properties of a series of ZrO_2-Gd_2O_3 alloys.

2. Experimental procedure

We have recently reported the preparation of tetragonal ZrO_2-Gd_2O_3 powders with good sinterability. Only the powders prepared by a coprecipitation route yielded a fully tetragonal phase and high sintered density. The mixed oxide and hybrid sol-gel routes of powder preparation lead to poor sintered density and only partial stabilization of the tetragonal phase. In the present work, we have therefore prepared the ZrO_2-Gd_2O_3 alloy powders by coprecipitation from Zr(iv) propoxide and $Gd(NO_3)_3.6H_2O$, as described in the earlier report [10]. The coprecipitated powders were washed in distilled water and propanol, dried at 120°C for 24 hours and calcined in air at 700°C for 4 hours. The calcined powders were mixed with a 1.5 wt% PVA solution, dried at 100°C, sieved through 75 mesh screen and uniaxially pressed at 220 MPa into either 15 mm $\phi \times 2.5$ mm high circular disks or $32 \times 12 \times 3$ mm rectangular bars. The green bodies were dried at 120°C, the binder was removed by heating the samples at 600°C for 30 minutes and sintering was carried out at 1400°C for 2 hours. Cooling was done at a rate of 3°C/min upto 750°C followed by furnace cooling.

The density of the sintered samples was determined using an x-ray diffractometer with Cu K_α radiation. The volume fraction V_m of the monoclinic (m) phase (talking the monoclinic and the tetragonal phases as the

basis) was obtained using the relations [11–13].

$$X_m = \frac{I_m(11\bar{1}) + I_m(111)}{I_m(11\bar{1}) + I_m(111) + I_t(111)}$$

and

$$V_m = \frac{PX_m}{1 + (P - 1(X_m))}$$

Here I_m and I_t denote the integrated peak intensities of the x-ray peaks for the monoclinic and the tetragonal phases for the indicated peak and P is a parameter whose value is usually between 1.29 and 1.34 [11, 12]. We have used $P = 1.31$ which is the value reported for Y-TZP [13].

For determining the relative amounts of t and cubic (c) phases, the x-ray data in the 2θ range 72°–76° was used. The relative amounts of t and c phases were obtained using the relations.

$$\frac{\nu_c}{\nu_t} = \frac{0.8745 I_c(400)}{I_t(400) + I_c(400)} \quad (1)$$

and

$$\nu_m + \nu_t + \nu_c = 1 \quad (2)$$

Here ν_c, ν_t and ν_m denote the volume fractions of the cubic, tetragonal and the monoclinic phases respectively. The factor 0.8745 in the above equation was calculated using the data given by Evans *et al.* [13], Klug and Alexander [14] and Cullity [15].

Lattice parameters of the tetragonal phase were determined using a least square fitting routine on a minimum of eight peaks.

Indentation fracture toughness K_{IC} was determined by indenting the samples with a Vickers indentor at 30 kg load and measuring toughness based on the method described by Anstis *et al.* [16]. Fracture toughness was also determined by three point bending of single edge notched beam (SENB) samples.

In order to limit the powder preparation efforts, small samples of size $12 \times 2.5 \times 0.85$ mm were used for strength measurement by three point bending with a span of 6.3 mm. However, in order to determine the variation in strength due to sample size, some selected compositions were also tested in four point bending using standard samples of size $25 \times 2 \times 1.5$ mm with inner and outer spans of 10 and 20 mm respectively [17]. The samples were polished on all sides to remove the surface layer of monoclinic zirconia prior to testing. At least 6 samples were used to determine each data point.

The extent of t → m transformation during fracture was determined by x-ray diffraction from the fracture surfaces of three point bend strength samples. The transformation depth d was determined using the relation [18].

$$d = \frac{\mathrm{Sin}\,\theta}{2\mu}\left[\frac{X_{meas} - X_{bulk}}{X_{surf} - X_{meas}}\right] \quad (3)$$

where X_{meas} and X_{bulk} are integrated x-ray intensity ratios of monoclinic ZrO_2 measured on the fracture surface and on the sintered sample respectively. X_{surf} is the same ratio for the very top layer of the fracture surface. As X_{surf} is not easily amenable to measurements its value is taken to be Y_{bulk}, the value for the transformable tetragonal phase in the bulk of the sample, i.e., it is assumed that all the transformable tetragonal phase is transformed at the top of the fracture surface. θ is taken to be 15° and μ is the linear absorption coefficient for x-rays.

Polished samples were thermally etched in air at 1350°C for 10 minutes and observed by SEM at 15 kV. The average grain size, D was calculated by the line intercept method using the relation by Mendelson [19].

$$D = 1.558\,L \quad (4)$$

where, L is the average intercept length over a large number of grains as measured on the plane of the polished surface. At least 200 grains were measured for each value of the average grain size. At higher concentrations of Gd_2O_3 (5 and 8 mol%), some grains distinctly larger than the others are present. For these two compositions, the average grain size was determined separately for the two types of grains.

3. Results

3.1. Phases

The phases in the sintered samples were determined in the composition range from 1.75 to 8 mol% as shown in Fig. 1. The data is from 4 to 5 samples and the bars show the scatter in the results. Michel *et al.* [6] found that a minimum of 3 mol% Gd_2O_3 is necessary to stabilize the tetragonal phase. However, in the present case we found this amount to be 2.5 mol% Gd_2O_3. Even with 1.75 mol% Gd_2O_3 only ~12 mol% monoclinic phase is present. The monoclinic content drops to 4 vol% with 2 mol% Gd_2O_3 while 2.5, 3 and 4 mol% samples are single phase tetragonal material. In 8 mol% samples the t phase peaks diminish while the peak due to c (400) becomes very sharp indicating that the major fraction of the specimen has cubic phase. The estimated volume percent of cubic phase in 5 and 8 mol% samples is 9 and 80% respectively.

3.2. Lattice parameter and *c/a* axial ratio

The change in the lattice parameter of the tetragonal phase with change in Gd_2O_3 content is shown in Fig. 2. The c axis shortens while the a axis elongates with

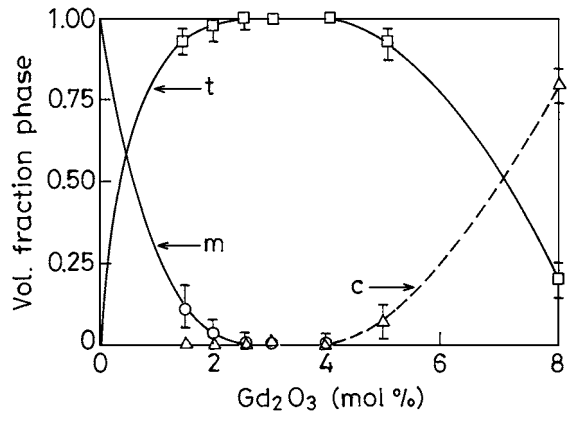

Figure 1 Phases in the sintered samples of ZrO_2-Gd_2O_3 alloys as a function of Gd_2O_3 content.

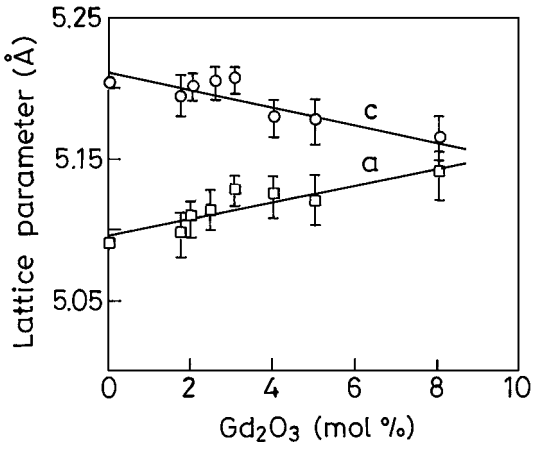

Figure 2 Lattice parameter of ZrO_2-Gd_2O_3 alloys.

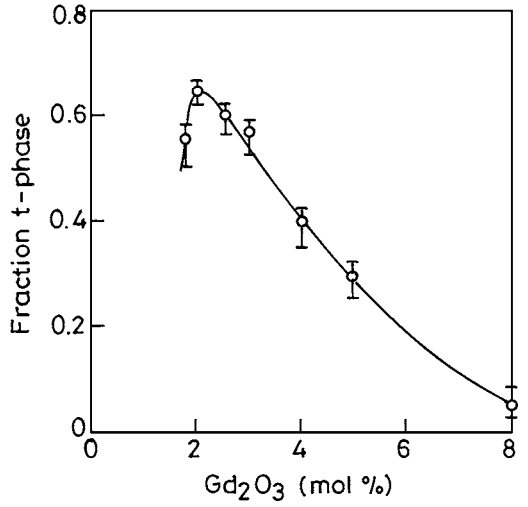

Figure 3 Tetragonal to monoclinic phase transformation on the fracture surface.

increasing Gd_2O_3 content. The lattice parameter for pure tetragonal phase with no Gd_2O_3 is taken from Sheu *et al.* [20]. A least square fit of the data indicates that c/a would become unity (i.e. a cubic phase would be obtained) at ~9.6 mol% Gd_2O_3.

3.3. Tetragonal to monoclinic transformation on fracture surface

Fraction of the tetragonal phase transformed to monoclinic phase on fracture surface is shown in Fig. 3. The extent of t → m transformation continuously decreases from 65% to ~5% with increase in Gd_2O_3 content from 2 to 8 mol%. The transformation zone depth decreases in a similar manner from 3.4 μm to 0.5 μm (Fig. 4). However, the extent of t → m transformation and the zone depth are smaller for 1.75 mol% Gd_2O_3 than for 2 mol% Gd_2O_3, giving a peak at 2 mol% Gd_2O_3.

3.4. Fracture toughness, strength and hardness

A peak in the fracture toughness is obtained at 2 mol% Gd_2O_3 (Fig. 5). Peak toughness is ~12 MPa $m^{1/2}$ for indentation method (Fig. 5a) and ~15 MPa $m^{1/2}$ for SENB samples (Fig. 5b). The measurement on SENB

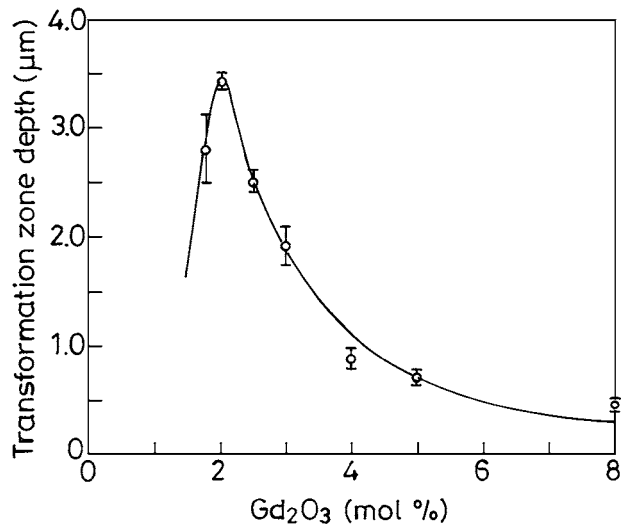

Figure 4 Transformation zone depth of ZrO_2-Gd_2O_3 alloys.

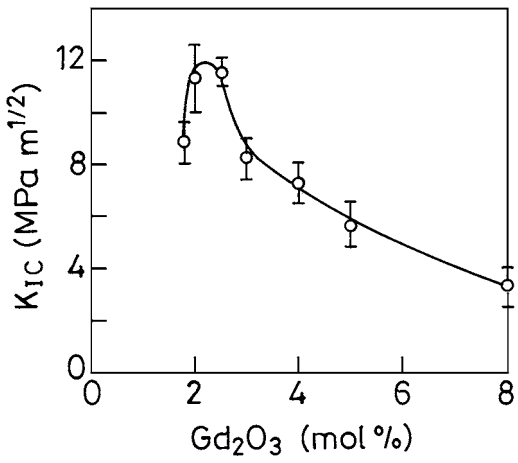

(a)

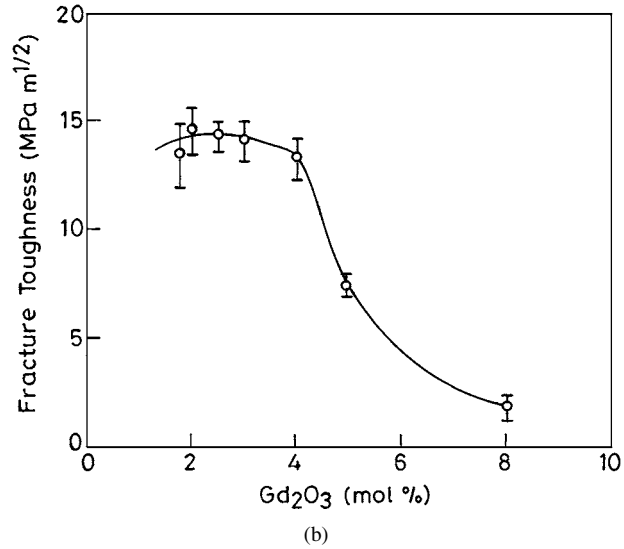

(b)

Figure 5 Fracture Toughness of ZrO_2-Gd_2O_3 alloys: (a) Indentation method, (b) SENB method.

samples is known to give an overestimate of K_{IC} due to a finite notch tip radius. For both methods fracture toughnes is ~10 MPa $m^{1/2}$ or more for Gd_2O_3 contents in the range 1.75–4 mol% Gd_2O_3 and decreases at higher Gd_2O_3 contents. The three point bend strength as a function of Gd_2O_3 content is shown in Fig. 6. Strength is maximum (~900 MPa) for 2–3 mol% Gd_2O_3. As

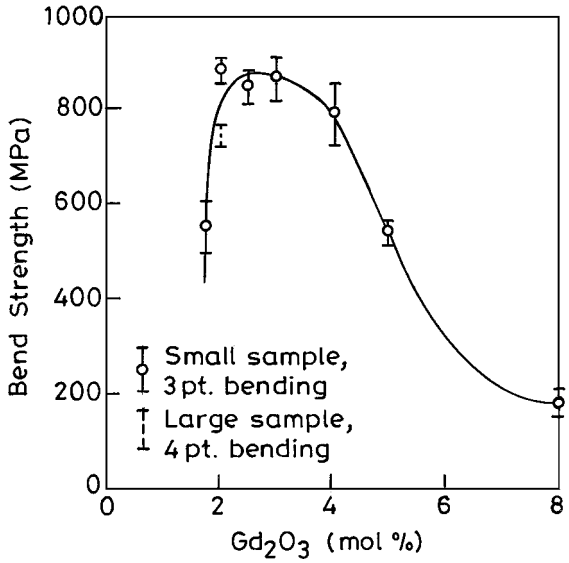

Figure 6 Three-point bend strength of ZrO_2-Gd_2O_3 alloys.

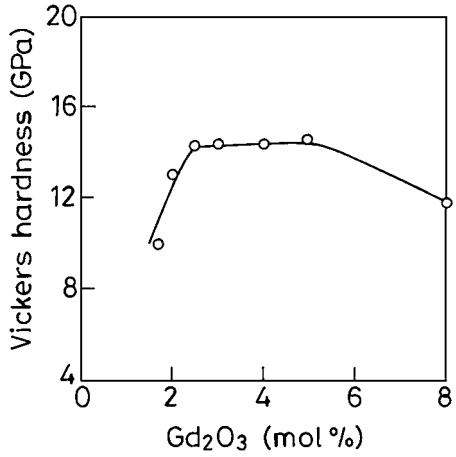

Figure 7 Vickers hardness of ZrO_2-Gd_2O_3 alloys.

a smaller than standard test sample size is used, the strength values are likely to be overestimated. Measurements on a few 2 mol% Gd_2O_3 samples using standard sized test bars as described earlier, showed that the overestimate is by about ~15% (Fig. 6). The hardness of the samples was obtained from the slope of the applied load (P) vs. square of the average value of half diagonal (a^2) for Vickers indentation. The maximum load used in these experiments was less than that at which the indentation cracks begin to form. The hardness H was calculated from the slope using the relation [21].

$$H = 0.47 \times \text{slope}$$

The variation in Vickers hardness with Gd_2O_3 content is shown in Fig. 7. There is a broad maximum in hardness (~14.2 GPa) for 2.5 to 5 mol% Gd_2O_3.

3.5. Density and microstructure

Fig. 8a to d show the microstructure of sintered ZrO_2-Gd_2O_3 samples. Except for 8 mol% Gd_2O_3 (Fig. 8d), grains in all the other samples are rounded and have extremely small size (0.10–0.15 μm). The grain size does not change much in the range 1.75 to 4 mol% Gd_2O_3. At 5 mol% a few large grains (0.3–0.4 μm) appear and at 8 mol% majority of the grains are large (~0.6 μm) (Fig. 9). These large grains, unlike the smaller grains are faceted i.e. they have sharp corners. The densities of the samples are given in Table I. Highest density (99% of the theoretical) is obtained at 3 mol% Gd_2O_3.

TABLE I Density of ZrO_2-Gd_2O_3 Alloys

Composition (mol% Gd_2O_3)	Relative density
1.75	0.90
2.0	0.92
2.5	0.93
3.0	0.99
4.0	0.96
5.0	0.92
8.0	0.88

4. Discussion

4.1. Effect of Gd_2O_3 on the phases

Several attempts have been made to determine the phase diagram of the ZrO_2-Gd_2O_3 system [22–25]. All of these including the more recent ones are confined to high temperatures ($\geq$1800°C), as compared to a sintering temperature of 1400°C in our experiments. A direct comparison of our results with these diagrams is therefore not possible. Furthermore, as pointed out by Leung *et al.* [7], the attainment of equilibrium in ZrO_2-Gd_2O_3 alloys is a slow process—it takes more than 200 hours at 1400°C to reach the equilibrium. Leung *et al.* found that a metastable tetragonal phase is obtained subsequent to precursor pyrolysis when Gd_2O_3 content is $\leq$6.5 mol%, which upon holding at high temperatures (1400°C), partitions into tetragonal and cubic phases. They estimated the maximum equilibrium solid solubility of Gd_2O_3 in tetragonal ZrO_2 to be 1.0 ± 0.1 mol% and minimum equilibrium solid solubility in cubic ZrO_2 to 8.0 ± 0.2 mol% at 1400°C. In the present experiments the samples were held at 1400°C for only 2 h as compared to 200 h used by Leung *et al.* [7]. Under these conditions, we find the solid solubility of Gd_2O_3 in the t phase to be as high as 4 mol% (Fig. 1). Similarly at $c/a = 1$, the solubility of Gd_2O_3 in cubic ZrO_2 is estimated to be 9.6 mol% (Fig. 2). This was verified by preparing two alloys containing 9 and 9.6 mol% Gd_2O_3—while some t phase was present in the former, the latter showed only the cubic phase. Similar results were also reported by Li *et al.* [25]. Clearly therefore, the phases in the present work are in metastable state, in view of the results of Leung *et al.*

The density data has been given in Table I. The variation in the sintered density (88–99%) with mol% Gd_2O_3 is quite large. Maximum density (99%) is obtained at 3 mol% Gd_2O_3 and much lower density ($\leq$90%) at the extreme values, 1.75 and 8 mol% Gd_2O_3.

The grain size remains nearly constant (0.10–0.15 μm) up to 4 mol% Gd_2O_3. At the higher Gd_2O_3 contents, larger grains are observed (Fig. 9). The presence of large grains at higher stabilizer content has been noted by many authors [7, 26]. This is because of the inhibition of the grain growth in the t-grain while the cubic phase shows no such inhibition. The large grains

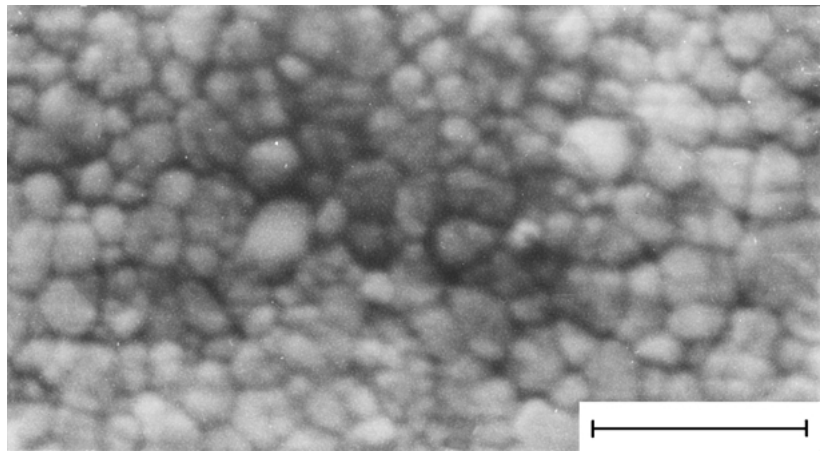

(a)

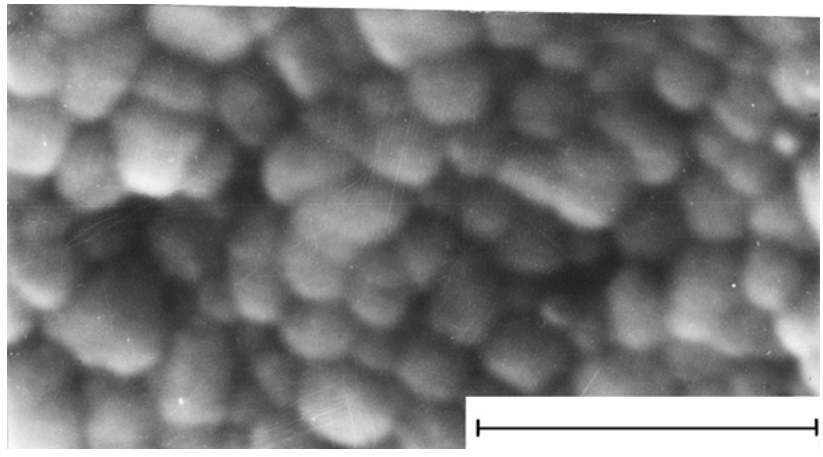

(b)

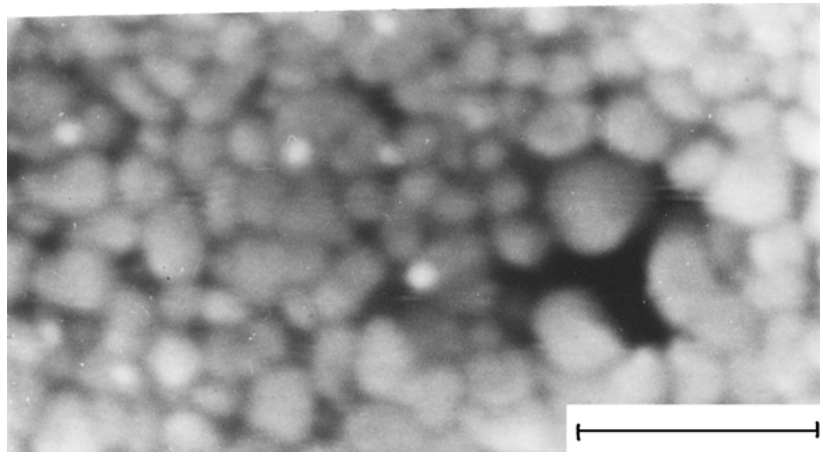

(c)

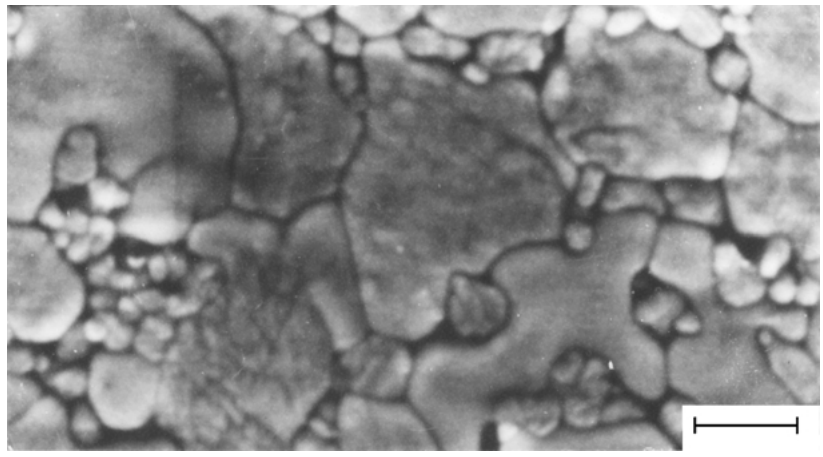

(d)

Figure 8 Microstructures of polished surfaces of ZrO_2-Gd_2O_3 alloys with increasing Gd_2O_3 concentration, (a) 1.75 mol%, (b) 3 mol%, (c) 5 mol% and (d) 8 mol%; the bar is 1 μm.

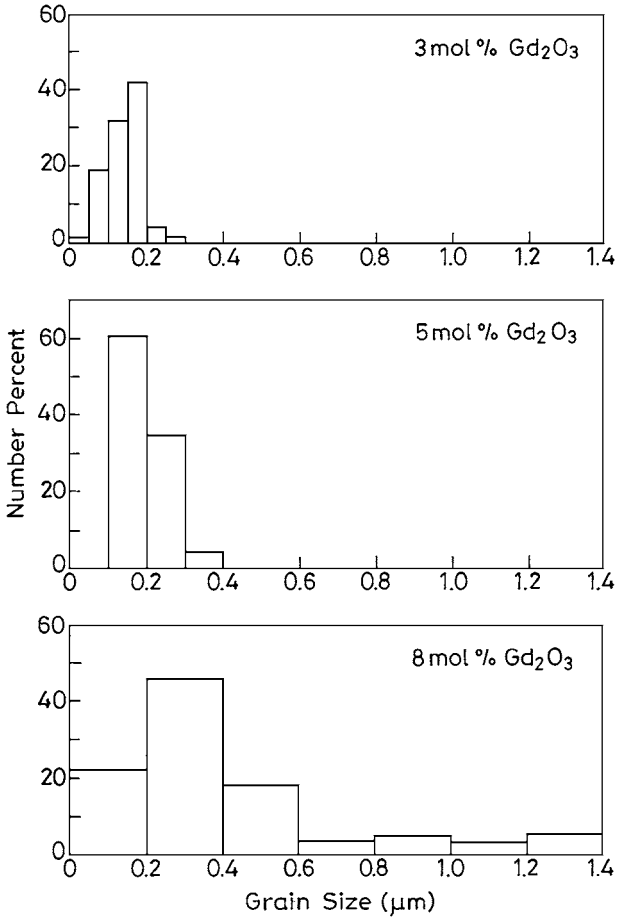

Figure 9 Grain Size distribution of ZrO_2-Gd_2O_3 alloys; the grain size distribution is nearly similar for Gd_2O_3 contents <3 mol%.

in these samples are most probably phase separated (cubic + tetragonal) grains. Various explanations have been proposed for the slow grain growth in the t phase. These are a solute drag model due to segregation of the stabilizer to the grain boundaries [27], space charge drag model [28] and coherency strains due to motion of boundaries between diffuse grains [29].

4.2. Fracture toughness

Variation in K_{IC} with mol% Gd_2O_3 is shown in Fig. 5. The maximum value of K_{IC} is ~12 MPa $m^{1/2}$ at 2 mol% Gd_2O_3 when measured by indentation method. The toughening in zirconia ceramics is mainly produced by the crack tip shielding mechanisms. These include transformation toughening and microcracking. Microcracking may become important when the ceramic contains a significant amount of the monoclinic phase. In the 1.75% sample, which has about ~12% m phase (the highest in all the samples), the toughness is not the highest. The other samples do not contain any m phase (except the 2% sample which has very small amount of the m phase). The microcracking accompanying the t to m transformation during cooling from the sintering temperature may be influencing the strength and hardness as discussed later. However, its contribution to toughness does not appear to be significant as compared to that due to transformation toughening. To quantify the contribution of transformation toughening (K_{ICTT}), the fraction of t phase transformed to m on the fracture

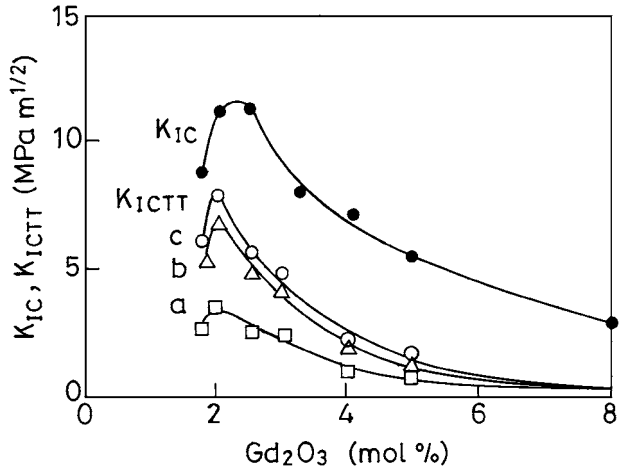

Figure 10 Plot of K_{IC} (experimental value) and K_{ICTT} (calculated) for (a) dilatation only, (b) shear only and (c) both dilatation and shear.

surface and the transformation zone depths were determined (Figs 3 and 4), K_{ICTT} was calculated using the following equations:

(a) Dilation only [30]

$$K_{ICTT} = \frac{0.22 E V_f e^T \sqrt{h}}{(1-\nu)} \tag{5}$$

(b) Shear only [30]

$$K_{ICTT} = 0.55 E V_f e^T \sqrt{h} \tag{6}$$

(c) Shear and dilation [31]

$$K_{ICTT} = \frac{0.48 E V_f e^T \sqrt{h}}{(1-\nu)} \tag{7}$$

In the above equations E is the Young's modulus, V_f is the volume fraction of the transformed phase, e_T is the transformation strain, h is the width of the transformation zone and ν is the Poisson's ratio.

The experimental values of K_{IC} and the K_{ICTT} calculated according to the above three equations are shown in Fig. 10. The largest contribution by transformation toughening is obtained when shear and dilation (equation 7 above) both are considered. This is able to account for most of the toughness. However, it should be noted that, to be precise, such calculation requires much more information [30] (such as the unconstrained transformation strain, elastic material of the material, particle size distribution, etc.) than is available.

The sources of the additional toughness could be (i) m → t reversal on the fracture surface after the passage of the crack; this would lead to an underestimate of the contribution due to transformation toughening (ii) domain switching in the tetragonal phase [32] and (iii) other effects like crack branching, microcracking etc. In order to determine whether there was any significant contribution to fracture toughness from domain switching, the ratios I(202)/I(220) and I(113)/I(131) for the t phase before and after transformation were examined. The reported values of these ratios for ZrO_2-CeO_2 alloys are shown in Table II [32] along with the

TABLE II Ratio of I(202)/I(220) and I(113)/I(131) from as sintered and on ground surface of ZrO_2-CeO_2 samples [Virkar *et al.*, ref. 32]

	Theoretical	As sintered	After surface grinding	% Relative change
I(202)/I(220)	2.0	2.16	8.21	+300
I(113)/I(131)	0.5	0.53	2.79	+460

measured values for ZrO_2-Gd_2O_3 which is reproduced in Table III. As seen from the tables the changes in intensity ratios are very small compared to those reported by Virkar *et al.* (Table II), and could be because of the texture which develops due to the t → m transformation during fracture [33, 34].

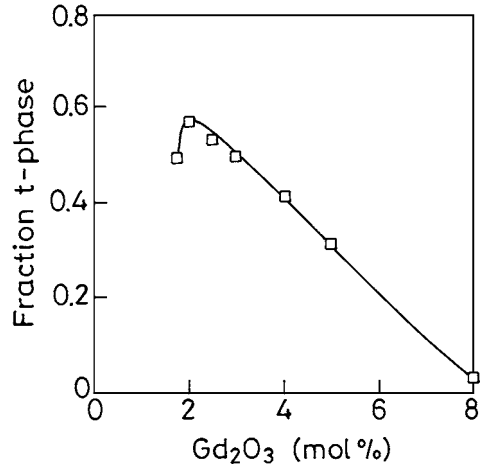

Figure 11 Fraction of the tetragonal phase that transformed to monoclinic by hand grinding of the samples.

4.3. Strength and hardness

In polycrystalline brittle materials the size of the strength determining flaw usually scales with the grain size. Very often a pore induces a microcrack along the grain boundaries and then the (pore + microcrack) acts as the critical flaw. The size of the critical flaw is thus expected to be larger in samples with large grains leading to a decrease in strength.

The histograms of grain size distribution for various samples are shown in Fig. 9. The expected correlation between the largest grain size and strength is observed only in samples with ≥4 mol% Gd_2O_3. These samples contain both tetragonal and cubic phases with the amount of cubic phase increasing with increasing Gd_2O_3 content. Thus it appears that failure in these samples initiates in the vicinity of the (cubic + tetragonal) grains, which have large size.

The strength of samples with ≤2 mol% Gd_2O_3 decreases as the amount of monoclinic phase increases. Microcrack formation usually occurs due to the volume expansion associated with t → m transformation during cooling and may be responsible for the observed degradation in strength. The strength in the single phase tetragonal region is nearly constant as is the size of largest grains.

As mentioned earlier, the measured strength values overestimate the actual strength due to small sample size. This is because the surface finishing operations used for preparing the samples for strength testing usually cause t – m transformation in the surface layer, producing compressive stresses on the surface. In the present experiments, the samples were hand polished. The amounts of the various phases, as shown earlier in Fig. 1, were determined from x-ray diffraction data from the polished surfaces. No m phase could be detected by x-ray diffraction in the samples having Gd_2O_3 content between 2.5 to 4 mol%. In a separate set of experiments, the fraction of the t phase that transforms to m phase on subjecting the sample to hand grinding was determined and is shown in Fig. 11. It can be seen that the hand grinding leads to significant transformation in the composition range 2 to 4 mol% Gd_2O_3. Absence of the m phase in the polished samples in this composition range thus shows that the t – m transformation due to polishing is negligible in our samples. Some transformation, not detectable by x-ray diffraction, does occur as evidenced by a slightly higher value of the strength for larger samples. However, even after taking this into account, the strength values compare favourably with the best reported for Y-TZP and Ce-TZP (800–900 MPa and 700–800 MPa respectively) [35, 36]. Optimization of processing should lead to further improvement in strength.

The hardness is found to be maximum and nearly constant between 2.5 to 5% Gd_2O_3 (Fig. 7). The tetragonal phase with strains due to tetragonal distortion is expected to have a higher hardness than the cubic phase. However, while c/a ratio continuously decreases as the Gd_2O_3 content is increased (Fig. 2) the hardness remains nearly constant in the composition range 2.5 to 5 mol%. Moreover, at 1.75 and 2 mol% Gd_2O_3, the hardness values are lower than maximum even though the c/a is nearly the highest and the phase is nearly fully tetragonal. This may have to do with the presence of small amounts of the monoclinic phase in these samples. It is possible that the formation of the m phase in the larger grains during cooling from the sintering temperature is accompanied by microcracks which contributes to the lowering of the hardness. The hardness is also influenced by porosity. However, in our case no correlation between the density and hardness are

TABLE III Ratio of I(202)/I(220) and I(113)/I(131) from as sintered and on fractured surface of ZrO_2-Gd_2O_3 alloys

Composition (mol% Gd_2O_3)	I(202)/I(220)			I(113)/I(131)		
	Polished	Fractured	% relative change	Polished	Fractured	% Relative change
3	2.16	1.61	−25.4	0.79	0.84	+6.3
4	2.52	1.75	−30.6	1.03	0.87	−15.1
5	3.44	3.00	−12.8	1.86	1.67	−9.1

observed indicating that the effect of the variation in density is not significant.

4.4. Dependence of tetragonal to monoclinic transformation on Gd_2O_3 content

The decrease in $t \rightarrow m$ transformation for $Gd_2O_3 <$ 2 mol% needs to be discussed (Fig. 3). In general, the $t \rightarrow m$ transformation should become thermodynamically easier as the stabilizer content decreases. However, if the $t \rightarrow m$ transformation is nucleation controlled, as appears to be the case [37, 38], then presence of second phase grains separating the tetragonal grains would also affect the total amount of $t \rightarrow m$ transformation. Such a microstructure suppresses the autocatalytic nucleation events and leads to a reduction in the fraction of transformed t phase. Thus the presence of about 10% monoclinic phase in 1.75 mol% Gd_2O_3 sample may be responsible for a decrease in the $t \rightarrow m$ transformation in these samples.

5. Summary

The tetragonal phase is formed in ZrO_2-Gd_2O_3 alloys containing 2 to 4 mol% Gd_2O_3 by sintering the samples prepared from coprecipitated poweders at 1400°C for 2 hours; the m and c phases appear at lower and higher Gd_2O_3 contents respectively.

The sintered density varies between 88 and 99%, the highest values being obtained at 3 mol% Gd_2O_3. The grain size is between 0.1 and 0.2 μm except in samples with higher (5 to 8 mol%) Gd_2O_3 where larger (cubic + tetragonal) grains are also present.

Maximum toughness of ~12 MPa $m^{1/2}$, as measued by indentation method, is found for 2 mol% Gd_2O_3 composition. The $t \rightarrow m$ transformation is also maximum at this composition. Transformation toughening is able to account for most of the toughness.

The samples with high toughness also have highest strength (~800 MPa measured on large samples) and hardness (14.2 GPa). The strength compares favourably with the best reported strength for Y-TZP and Ce-TZP. Further improvement in strength should be possible with improved processing.

Acknowledgment

This research was partially funded by a grant from Council of Scientific Industrial Research, Government of India.

References

1. T. SATO, S. OHTAKI, T. ENDO and M. SHIMADA, *J. Amer. Ceram. Soc.* **68** (1985) C-320.
2. S. MASCHIO, E. BISCHOFF, O. SBAIZERO and S. MERIANI, *J. Mater. Sci.* **27** (1992) 2734.
3. T. VAN DIJK and A. J. BURGGRAFF, *Phys. Status Solidi* A **58** (1980) 115.
4. F. MOZTARZADEH, in "Advances in Ceramics," Vol. 24B: Science and Technology of Zirconia III, edited by S. Somiya, N. Yamamoto and H. Yanagida (American Ceramic Society, Westerville, OH. 1988) p. 901.
5. T. K. KANG, T. NAGASAKI, N. IGAWA, K. I-HIUN and H. OHNO, *J. Amer. Ceram. Soc.* **75** (1993) 2297.
6. D. MICHEL, L. MAZEROLLES and M. PEREZ Y. JORBA, *J. Mater. Sci.* **18** (1983) 2618.
7. D. K. LEUNG, C. J. CHAN, M. RUHLE and F. F. LANGE, *J. Amer. Ceram. Soc.* **74** (1991) 2786.
8. M. YOSHIMURA, *Am. Ceram. Soc. Bull.* **67** (1988) 1950.
9. J. EMSELY, "The Elements" (Oxford University Press, Oxford, 1988).
10. S. BHATTACHARYYA and D. C. AGARWAL, *J. Mater. Sci.* **30** (1995) 1495.
11. H. TORAYA, M. YOSHIMURA and S. SOMIYA, *J. Amer. Ceram. Soc.* **67** (1984) C-119.
12. H. K. SCHMID, *ibid.* **70** (1987) 367.
13. P. A. EVANS, R. STEVENS and J. G. P. BINNER, *Trans. J. Brit. Ceram. Soc.* **83** (1984) 39.
14. H. P. KLUG and L. E. ALEXANDER, "X-ray Diffraction Procedures for Polycrystalline and Amorphous Materials," 2nd ed. (John Wiley, New York, 1974) p. 880.
15. B. D. CULLITY, "Elements of X-ray Diffraction" (Addison-Wesley Publishing Company, Massachusetts, 1977) p. 520.
16. G. R. ANSTIS, P. CHANTIKUL, B. R. LAWN and D. B. MARSHALL, *J. Amer. Ceram. Soc.* **64** (1981) 533.
17. G. D. QUINN and R. MORELL, *ibid.* **74** (1991) 2037.
18. Y. MORI, Y. KITANO, A. ISHITANI and T. MASAKI, *ibid.* **71** (1988) C-322.
19. M. I. MENDELSON, *ibid.* **52** (1969) 443.
20. T. S. SHEU, T.-Y. TIEN and I.-W. CHEN, *ibid.* **75** (1992) 1108.
21. A. G. EVANS and E. A. CHARLES, *ibid.* **59** (1976) 371.
22. M. PEREZ and Y. JORBA, *Ann. Chim. (Paris)* **7** (1962) 509.
23. J. LEFEVRE, *ibid.* **8** (1963) 128.
24. A. ROUANET and M. FOEX, in "Phase Diagrams for Ceramists, 1975 Supplement," edited by E. M. Levin and H. F. McMurdie (American Ceramic Society Inc., Westerville, OH) Fig. 4417.
25. P. LI, I. W-CHEN and J. E. PENNER - HAHN, *J. Amer. Ceram. Soc.* **77** (1994) 118.
26. F. F. LANGE, *ibid.* **69** (1986) 240.
27. G. S. A. U. THEUNISSEN, A. J. A. WINNUBUST and A. J. BURGRAAF, *J. Mater. Sci. Lett.* **8** (1989) 55.
28. S. L. HUANG and I.-W. CHEN, *J. Amer. Ceram. Soc.* **73** (1990) 3269.
29. F. F. LANGE, D. B. MARSHALL and J. R. PORTER, in "Ultrastructue Processing of Ceramics, Glasses and Composites," edited by J. D. Mackenzie and D. R. Ulrich (Wiley, New York, 1988) p. 519.
30. R. M. McMEEKING and A. G. EVANS, *J. Amer. Ceram. Soc.* **65** (1982) 242.
31. P. E. REYES-MOREL and I-WEI CHEN, *ibid.* **71** (1988) 343.
32. A. V. VIRKAR and R. L. K. MATSUMOTO, *ibid.* **69** (1986) C-224.
33. K. J. BOWMAN, *ibid.* **74** (1994) 2690.
34. K. J. BOWMAN and I. W. – CHEN, *ibid.* **76** (1993) 113.
35. K. TSUKUMA, Y. KUBOTA and T. TSUKIDATE, in "Advances in Ceramics," Vol. 12, edited by N. Claussen, M. Ruhle and A. H. Heuer (American Ceramic Society, Columbus, OH, 1984). p. 382.
36. K. TSUKUMA and M. SHIMADA, *J. Mater. Sci.* **20** (1985) 1178.
37. I.-WEI CHEN and Y.-H. CHIAO, in "Advances in Ceramics Vol. 12: Science and Technology of Zirconia II, edited by N. Claussen, M. Ruhle and A. H. Heuer (American Ceramic Society, Columbus, OH, 1984) p. 33.
38. I-WEI CHEN and Y. H. CHIAO, *Acta. Metall.* **33** 9(1985) 1827.

Received 28 November 2000
and accepted 21 November 2001